Monthly Notices
of the
ROYAL ASTRONOMICAL SOCIETY

MNRAS **495,** L81–L85 (2020)
Advance Access publication 2020 April 26

doi:10.1093/mnrasl/slaa063

Cosmic archaeology with massive stellar black hole binaries

L. Graziani [1,2,3★] R. Schneider [1,2,4] S. Marassi,[1,2] W. Del Pozzo [5] M. Mapelli [6,7,8] and N. Giacobbo [6,7,8]

[1]*Dipartimento di Fisica, Sapienza, Università di Roma, Piazzale Aldo Moro 5, I-00185 Roma, Italy*
[2]*INFN, Sezione di Roma I, P.le Aldo Moro 2, I-00185 Roma, Italy*
[3]*INAF/Osservatorio Astrofisico di Arcetri, Largo E. Femi 5, I-50125 Firenze, Italy*
[4]*INAF/Osservatorio Astronomico di Roma, Via di Frascati 33, I-00078 Monte Porzio Catone, Italy*
[5]*Dipartimento di Fisica 'Enrico Fermi', Università di Pisa, I-56127 Pisa, Italy*
[6]*Dipartimento di Fisica e Astronomia 'G. Galilei', Università di Padova, vicolo dell'Osservatorio 3, I-35122 Padova, Italy*
[7]*INFN, Sezione di Padova, Via Marzolo 8, I-35131 Padova, Italy*
[8]*INAF/Osservatorio Astronomico di Padova, Vicolo dell' Osservatorio 5, I-35122 Padova, Italy*

Accepted 2020 April 7. Received 2020 March 29; in original form 2020 January 30

ABSTRACT

The existence of massive stellar black hole binaries (MBHBs), with primary black hole masses $\geq 31\,M_\odot$, was proven by the detection of the gravitational wave (GW) event GW150914 during the first LIGO/Virgo observing run (O1), and successively confirmed by seven additional GW signals discovered in the O1 and O2 data. By adopting the galaxy formation model GAMESH coupled with binary population synthesis (BPS) calculations, here we investigate the origin of these MBHBs by selecting simulated binaries compatible in mass and coalescence redshifts. We find that their cosmic birth rates peak in the redshift range $6.5 \leq z \leq 10$, regardless of the adopted BPS. These MBHBs are then old systems forming in low-metallicity ($Z \sim [0.01–0.1]\,Z_\odot$), low-stellar-mass galaxies, before the end of cosmic reionization, i.e. significantly beyond the peak of cosmic star formation. GW signals generated by coalescing MBHBs open up new possibilities to probe the nature of stellar populations in remote galaxies, at present too faint to be detected by available electromagnetic facilities.

Key words: gravitational waves – stars: black holes – Galaxy: evolution – Galaxy: formation – Galaxy: stellar content – cosmology: theory.

1 INTRODUCTION

Since the discovery of the first gravitational wave (GW) signal GW150914 (Abbott et al. 2016) and to date, the LIGO/Virgo Collaboration detected four events interpreted as originated by the coalescence of massive stellar black hole binaries (MBHBs; i.e. systems with $m_1 \in [31, 66]\,M_\odot$, $m_2 \in [21, 43]\,M_\odot$) at a median luminosity distance $d_L \geq 440$ Gpc (Abbott et al. 2019a); interestingly enough, a recent independent data analysis (Venumadhav et al. 2019) expanded the above sample with four new systems (see Table 1). Even more intriguing, the current O3 run has already reported more than 14 alerts with similarly high d_L.[1]

Future ground-based interferometers such as KAGRA (Akutsu et al. 2019) and LIGO-India will join the global GW detector network improving the event localization up to 90 per cent confidence (Abbott et al. 2018). Space-based missions will target the mHz band with LISA[2] and the dHz band with DECIGO.[3] This synergistic multiband approach (Sesana 2016) will place better constraints on MBHBs, also accessing their early inspiral phases (Isoyama, Nakano & Nakamura 2018). Finally, 3G detectors such as the Einstein Telescope[4] and Cosmic Explorer[5] could detect stellar MBHBs up to extremely high redshifts (Kalogera et al. 2019).

Stellar models predict MBHBs to be the end products of metal-poor stars (Mapelli, Colpi & Zampieri 2009; Belczynski et al. 2010; Mapelli et al. 2010; Spera, Mapelli & Bressan 2015). Given our current understanding of galaxy evolution, these stars are preferentially formed in low-mass and less chemically evolved galaxies (Maiolino & Mannucci 2019), hardly resolved by large-scale cosmological simulations.

Binary population synthesis (BPS) codes are traditionally adopted to investigate the evolution of black hole (BH) binaries

★ E-mail: luca.graziani@roma1.infn.it

[1]https://gracedb.ligo.org/latest/

[2]https://www.elisascience.org/
[3]http://tamago.mtk.nao.ac.jp/decigo/
[4]http://www.et-gw.eu/
[5]https://cosmicexplorer.org/

Table 1. Properties of the GW events (in column) associated with the MBHBs found in O1 and O2 (Abbott et al. 2019a) and extended by Venumadhav et al. (2019) (although with lower $p_{\rm astro}$ and FAR values, GW IDs in bold). Each row shows source frame component masses m_1 and m_2, chirp mass $\mathcal{M}$, final source frame mass $M_{\rm f}$, luminosity distance $d_{\rm L}$, estimated coalescence redshift $z_{\rm c}$, and estimated coalescence rates ($\mathcal{R}$ [cGpc^{-3} yr^{-1}]) predicted by SEBA/MOBSE in our Local Group-like volume of 4^3 cMpc^3.

	GW150914	GW170729	GW170818	GW170823	**GW170304**	**GW170403**	**GW170425**	**GW170727**
$m_1/{\rm M}_\odot$	$35.6^{+4.8}_{-3.0}$	$50.2^{+16.2}_{-10.2}$	$35.4^{+7.5}_{-4.7}$	$39.5^{+11.2}_{-6.7}$	$41.0^{+12.0}_{-7.0}$	$44.0^{+12.0}_{-8.0}$	$44.0^{+19.0}_{-10.0}$	$39.0^{+10.0}_{-6.0}$
$m_2/{\rm M}_\odot$	$30.6^{+3.0}_{-4.4}$	$34.0^{+9.1}_{-10.1}$	$26.7^{+4.3}_{-5.2}$	$29.4^{+6.7}_{-7.8}$	$31.0^{+7.0}_{-8.0}$	$32.0^{+8.0}_{-9.0}$	$29.0^{+11.0}_{-8.0}$	$29.0^{+6.0}_{-7.0}$
$\mathcal{M}/{\rm M}_\odot$	$28.6^{+1.7}_{-1.5}$	$35.4^{+6.5}_{-4.8}$	$26.5^{+2.1}_{-1.7}$	$29.2^{+4.6}_{-3.6}$	$47.0^{+8.0}_{-7.0}$	$48.0^{+9.0}_{-7.0}$	$47.0^{+26.0}_{-10.0}$	$42.0^{+6.0}_{-6.0}$
$M_{\rm f}/{\rm M}_\odot$	$63.1^{+3.4}_{-3.0}$	$79.5^{+14.7}_{-10.2}$	$59.4^{+4.9}_{-3.8}$	$65.4^{+10.1}_{-7.4}$				
$d_{\rm L}/{\rm Mpc}$	440^{+150}_{-170}	2840^{+1400}_{-1360}	1060^{+420}_{-380}	1940^{+970}_{-900}				
$z_{\rm c}$	$0.09^{+0.03}_{-0.03}$	$0.49^{+0.19}_{-0.21}$	$0.21^{+0.07}_{-0.07}$	$0.35^{+0.15}_{-0.15}$	$0.50^{+0.2}_{-0.2}$	$0.45^{+0.22}_{-0.19}$	$0.50^{+0.4}_{-0.3}$	$0.43^{+0.17}_{-0.17}$
$\mathcal{R}$ (SEBA/MOBSE)	2.01/87.26	0.06/6.81	5.23/124.90	5.65/111.10	7.14/52.34	6.99/49.12	7.38/108.63	6.37/112.39

by generating data bases (DBs) from distributions of initial stellar masses and orbital parameters. By coupling them with estimates of the cosmic star formation rate (SFR) and of the average metallicity evolution (or mass–metallicity relation), their coalescence rates along z can be inferred (Marassi, Schneider & Ferrari 2009; Schneider, Marassi & Ferrari 2010; Marassi et al. 2011; Regimbau 2011; Dominik et al. 2013; Belczynski et al. 2016; Dvorkin et al. 2016; Lamberts et al. 2016; Elbert, Bullock & Kaplinghat 2018; Bavera et al. 2020; Chruslinska, Nelemans & Belczynski 2019; Neijssel et al. 2019). With hydrodynamic simulations or semi-analytic models (SAMs), the cosmological evolution of compact binaries can be studied connecting galaxies hosting their birth and coalescence (Mapelli et al. 2017; O'Shaughnessy et al. 2017; Schneider et al. 2017; Mapelli & Giacobbo 2018; Artale et al. 2019; Marassi et al. 2019).

Here, we use the GAMESH model to predict the origin of MBHBs in a Local Group-like volume. In Schneider et al. (2017), we already investigated the birth and coalescence sites of compact binaries generating O1 GW events, while in Marassi et al. (2019) we looked at observational counterparts of GW150914 hosts. Here, we go one step forward by exploring the birth and coalescence of the MBHBs in Table 1, with an increased statistical sample of massive binaries and by comparing predictions of two independent BPS DBs: SEBA (Portegies Zwart & Verbunt 1996; Mapelli et al. 2013) and MOBSE (Giacobbo, Mapelli & Spera 2018).

We provide the statistical evidence that the highest birth rate of their stellar progenitors is found in low-metallicity ($Z \leq 0.1$ Z$_\odot$), star-forming dwarf galaxies living in the redshift range $6.5 \leq z \leq 10$, i.e. in the epoch of reionization (EoR, $z \geq 6$). While this result is proven to be independent of the adopted BPS, the number of coalescence events strongly depends on the prescriptions implemented in binary evolution codes for massive BH formation.

2 GALAXY FORMATION MODEL

GAMESH (Graziani et al. 2015, 2017; Graziani 2019) is a galaxy formation model based on a hybrid pipeline combining a dark matter (DM)-only simulation, an SAM for star formation and chemical evolution, and a radiative transfer module. The DM run simulates a multizoom cosmic box better resolved in its inner cubic volume of 4^3 cubic comoving megaparsecs (cMpc^3), centred on a Milky Way-like halo (a Local Group-like volume). The SAM module runs on a galaxy catalogue taken from a larger volume ($\sim 8^3$ cMpc^3) to capture a wider statistics of intermediate/dwarf galaxies whose stellar and chemical evolution in $0 < z < 20$ is regulated by two parameters: star formation and wind efficiency. The resulting baryonic properties of the MW are in agreement with observations. Moreover, the histories of a plethora of well-resolved dwarf galaxies, coevolving under strong dynamical interactions and feedback,[6] naturally reproduce observed galaxy scaling relations (Graziani et al. 2017; Ginolfi et al. 2018). In Schneider et al. (2017), GAMESH was extended to self-consistently account for compact binary systems by assigning a binary fraction of $f_{2,*} = 1$ and by randomly sampling the newly formed stellar mass with a SEBA DB having 2×10^6 binaries in the initial mass function (IMF) mass range $M_\star \in [0.01, 100]$ M$_\odot$. Here, we adopt two new independent DBs improving the statistics of MBHBs: a MOBSE DB with 10^7 binaries sampling $M_\star \in [5.0, 150]$ and a SEBA DB with 2×10^7 systems in $M_\star \in [8.0, 100]$. Each DB has 12 metallicity bins, regularly spanning the range $Z \in [0.01, 1]$ Z$_\odot$.[7] While the two BPS assume the same stellar evolutionary tracks and metallicity-dependent mass-loss in stellar winds,[8] the stellar evolution channels producing massive BHs are significantly different: the MOBSE $\alpha 5$ run adopts the rapid SN model of Fryer et al. (2012), while in SEBA all stars with pre-SN masses $m_{\rm pre,SN} \geq 40$ M$_\odot$ are assumed to collapse into a BH with no SN explosion; the resulting BH mass is then $m_{\rm BH} = m_{\rm CO} + (2/3)(m_{\rm He} + m_{\rm H})$ (Mapelli et al. 2013). The common envelope (CE) efficiencies also differ: $\alpha = 1.0$, $\lambda = 0.5$ in SEBA, while in MOBSE $\alpha = 5$ and λ depends on the stellar type. Note that these parameters critically affect the statistics of low-mass BHBs but have a minor impact on the merger rate of MBHBs (Giacobbo et al. 2018).

Once the newly formed $M_\star$ in each galaxy is populated with binaries randomly sampled from the DB with Z closest to the stellar metallicity $Z_\star$, we follow them in time from their birth (t_0) to

[6]Here radiative feedback is implemented by assuming that the volume instantly reionizes at $z = 6$.

[7]For details on the set-up of the two DBs, please refer to the $\alpha 5$ run of Giacobbo & Mapelli (2018) and to Schneider et al. (2017). We also assume Z$_\odot = 0.02$. Finally note that the prescriptions in MOBSE and SEBA are not tailored to describe systems to describe systems with $Z < 0.01$ Z$_\odot$ and we are forced to extrapolate the results of $Z = 0.01$ Z$_\odot$ at lower metallicities, with a possible impact on the results, especially for galaxies hosting Pop III stars.

[8]In MOBSE, the metallicity dependence is also suppressed when the electron scattering Eddington factor $\Gamma_{\rm e} \geq 2/3$ (Giacobbo et al. 2018).

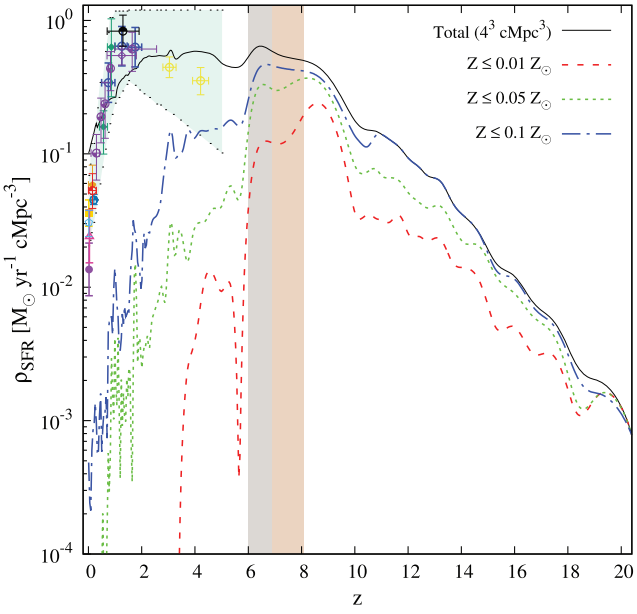

Figure 1. SFR density as a function of redshift z in the $(4\ \mathrm{cMpc})^3$ volume: total (solid black), from galaxies with $Z_\star \leq 0.01\ Z_\odot$ (dashed red line), $Z_\star \leq 0.05\ Z_\odot$ (dotted green), and $Z_\star \leq 0.1\ Z_\odot$ in dot–dashed blue line. Shaded areas indicate the redshift range of the reionization midpoint $6.9 < z_{50\ \mathrm{per\ cent}} < 8.1$ (light pink; Planck Collaboration VI 2018) and the assumed end of reionization (grey). Observational data and its general level of uncertainty in the Local Volume (cyan shaded area) are collected from Hopkins, Irwin & Connolly (2001).

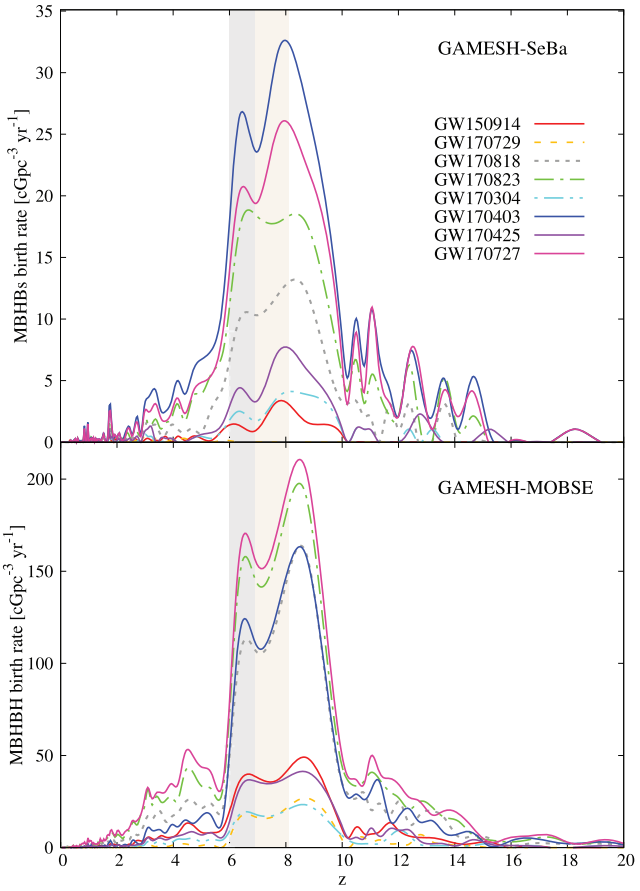

Figure 2. Birth rates (cGpc^{-3} yr^{-1}) of our MBHBs stellar progenitors as a function of redshift z. The two panels adopt the same galaxy formation model but different BPS calculations: SEBA (top) and MOBSE (bottom). The light pink and grey shaded areas are the same as in Fig. 1.

coalescence (t_c), by relating ancestors with descendant galaxies. In Fig. 1, we show the predicted total SFR density ρ_{SFR} as a function of redshift (solid black line). Dashed red, dotted green, and dash–dotted blue lines correspond to the same quantity computed by summing up the contributions of star-forming galaxies with $Z_\star \leq 0.01$, and 0.05, 0.1 $Z_\odot$, respectively. The simulated trend is in very good agreement with the observational data at $z < 4$ and their range of uncertainty, collected from Hopkins et al. (2001). Noticeably, systems with $Z \leq 0.05\ Z_\odot$ provide a major contribution to ρ_{SFR} from the cosmic dawn ($z \sim 18$) down to $z \sim 6$, making small, normal star-forming galaxies (see Graziani et al. 2020 for a definition) the dominant population at these epochs. Gas photoheating associated with cosmic reionization progressively diminishes their contribution (see the relative drops in red/green/blue lines) until the total SFR becomes sustained only by intermediate-mass galaxies hosted in Lyα-cooling haloes at $z < 6$ (Graziani et al. 2015).

3 RESULTS

Before presenting our results, we note here that MBHBs are identified in the simulation by requiring that both masses, m_1, m_2, and coalescence redshift z_c (derived from t_c) lie within the observational uncertainties reported in Table 1.

3.1 MBHB formation sites and birth rates

The birth rates of stellar progenitors evolving into the selected MBHBs are shown in Fig. 2, as a function of z; top/bottom panels show rates obtained coupling with SEBA/MOBSE with identical line styles and colours for the same GW signal. It is immediately evident that all birth rates peak in the redshift range $6.5 \leq z \leq 10$ regardless of the adopted BPS, and that their shape is similar across GW signals, reflecting the underlying SFR(z) trend.[9] The absolute values for each signal, on the other hand, strongly vary across BPS predictions as well as their relative height and line shapes (see also Section 3.2). The coalescence rate of each MBHB is provided in the last row of Table 1, while the total merger rates (i.e. when all binary BHs in the simulation are considered, regardless of their masses) at $z = 0.2$ and $z = 0$ are $\mathcal{R}_0 = 4195\ (1513)$ Gpc^{-3} yr^{-1} and $\mathcal{R}_{0.2} = 5564\ (1584)$ Gpc^{-3} yr^{-1} for SEBA (MOBSE); consequently, our MBHBs contribute only for 7 (41) per cent to the total value at $z = 0$.

While a direct comparison with observationally inferred rates [24.4–140.4] Gpc^{-3} yr^{-1} (Abbott et al. 2019b) is not feasible because Local Group-like volumes are generally overdense and

[9]This result is peculiar of the selected massive binaries. A broader mass selection extending to lower BH masses would shift their birth rates closer to the SFR peak. Moreover, our previous results (Schneider et al. 2017), while based on the same cosmological run, did not have enough statistical sampling of the high-mass end of the stellar initial mass function and therefore underestimated the birth rates of GW150914-like events in low-mass, low-metallicity galaxies at high z (see Section 2). Finally, the results are also confirmed by Monte Carlo convergence tests performed with different random number chains.

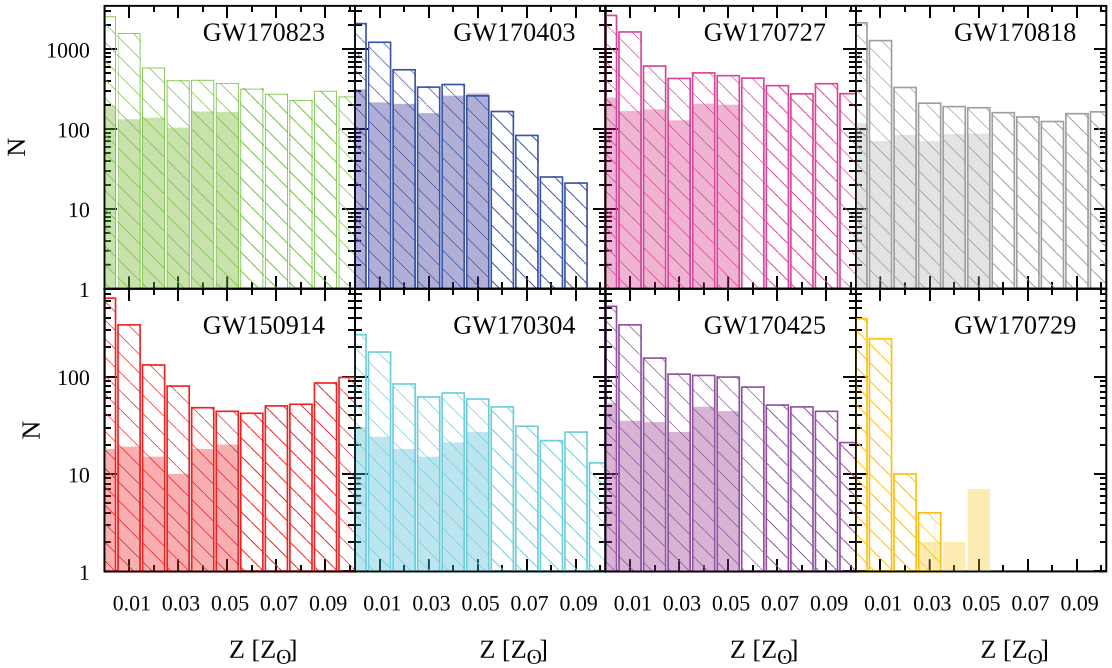

Figure 3. Total number of GW events (N, in logarithmic scale) predicted to form at each Z by SEBA (filled histograms) and MOBSE (dashed histograms) run on the same galaxy formation model. Each panel represents the results obtained for individual GW events and the colour coding is the same as in Fig. 2.

then not representative of larger cosmological scales,[10] we note that Mapelli et al. (2017) adopted the same MOBSE DB on the Illustris simulation (with a cubic box size of $L_{\rm box} = 106.5$ cMpc) finding $\mathcal{R}_0 = 155\ {\rm Gpc^{-3}\ yr^{-1}}$ and $\mathcal{R}_{0.2} = 228\ {\rm Gpc^{-3}\ yr^{-1}}$, close to the 90 per cent credible values of Abbott et al. (2019b). However, the contribution of high-z dwarfs remains mostly undetermined in large cosmological simulations and in models that adopt observationally inferred scaling relations, such as the mass–metallicity relation and galaxy main sequence, which are not yet observed at $z \geq 6$.

3.2 Metallicity dependence

The distribution in metallicity of MBHBs stellar progenitors is shown in Fig. 3; filled (dashed) histograms show the results obtained with SEBA (MOBSE). All the stellar progenitors predicted with the SEBA DB form at metallicity $Z \leq 0.05\ {\rm Z_\odot}$ following a nearly flat distribution,[11] while MOBSE predictions involve higher gas metallicity, up to $Z = 0.1\ {\rm Z_\odot}$. Also note that the percentage of binaries with $Z \leq 0.05\ {\rm Z_\odot}$ is always higher than 66 per cent for all the GW events. As the SFR in $6 \leq z \leq 10$ is largely dominated by galaxies with $Z \leq 0.05\ {\rm Z_\odot}$ (see Fig. 1), MBHB birth rates show the highest peak in this redshift range independently of the adopted BPS. The discrepancy in their absolute values reflects differences in the two BPS. In all metallicity bins, the number of MBHBs predicted by MOBSE largely exceeds the one of SEBA, reflecting the assumptions made on how massive BHs form. MBHBs predicted by MOBSE at $Z > 0.05\ {\rm Z_\odot}$ also originate from very massive progenitors: GW150914-like systems with $Z \geq 0.08\ {\rm Z_\odot}$, for example, have primary stars with $m_1 > 100\ {\rm M_\odot}$ with sufficiently massive CO core, at the pre-SN stage, to meet the conditions of direct BH collapse, despite their mass-loss (Fryer et al. 2012). Such BHs are not formed by SEBA, either because the IMF of the primary star does not extend beyond $100\ {\rm M_\odot}$ or because efficient mass-loss reduces their pre-SN mass below the $40\ {\rm M_\odot}$ limit, necessary for direct BH formation. Finally, it is important to stress that the histograms in Fig. 3 result from the convolution of the intrinsic BPS metallicity distribution functions and the way metallicity-dependent formation sites evolve in the cosmological simulation. Hence, these findings indicate that both BPS models predict a fraction of MBHBs to form with large orbital separations, delaying their merger by 8–12 Gyr since the formation.

4 CONCLUSIONS

In this paper, we investigate the origin of the most MBHBs ($m_1 \geq 31\ {\rm M_\odot}$) detected during the LIGO/Virgo O1 and O2 runs (see Table 1). By running the galaxy evolution model GAMESH coupled with SEBA and MOBSE BPS calculations, we select binaries with primary and secondary masses and coalescence redshift within the observed ranges, and establish their cosmological birth rate and the successive redshift evolution. We find that all birth rates peak in the redshift range $6.5 \leq z \leq 10$, i.e. before the end of cosmic reionization, regardless of the BPS model.

Three conditions act in concert to provide this result: (i) a large number of star-forming dwarf galaxies contribute to the total SFR in the EoR; (ii) their chemical evolution leaves the gas metallicity below $Z \approx 0.1\ {\rm Z_\odot}$; and (iii) the statistics of coalescence times of MBHBs under investigation peak at very high values ($t_{\rm c} > 9.5$ Gyr) allowing them to merge in the interval of $z_{\rm c}$ inferred from the detected GW signals (Belczynski et al. 2016; Mapelli et al. 2019).

[10]The $\rho_{\rm SFR}$ shown in Fig. 1 is approximately one order of magnitude larger than the cosmic SFR density at $z < 4$ (Madau & Fragos 2017) and flatter at higher z.

[11]For GW170729, the most massive among the MBHB sample shown in Table 1, the number of systems predicted by SEBA is 32, i.e. too small to appear in the log scale adopted in 3. All these systems, however, form at $Z \leq 0.02\ {\rm Z_\odot}$.

Hence, we predict these MBHBs to preferentially form in low-metallicity, star-forming dwarfs at redshifts significantly higher than the peak of cosmic star formation that are hardly resolved in large-scale cosmological simulations and that are beyond the observational capabilities of current electromagnetic facilities. Future GW and electromagnetic facilities will be able to improve our knowledge of these ancient systems, fully exploiting their potential as cosmic archaeology probes.

ACKNOWLEDGEMENTS

LG and RS acknowledge support from the Amaldi Research Center funded by the MIUR program 'Dipartimento di Eccellenza' (CUP:B81I18001170001). MM and NG acknowledge financial support by the European Research Council for the ERC Consolidator grant DEMOBLACK, under contract no. 770017.

REFERENCES

Abbott B. P. et al., 2016, Phys. Rev. Lett., 116, 061102
Abbott B. P. et al., 2018, Living Rev. Relativ., 21, 3
Abbott B. P. et al., 2019a, Phys. Rev. X, 9, 031040
Abbott B. P. et al., 2019b, ApJ, 882, L24
Akutsu T. et al., 2019, Nat. Astron., 3, 35
Artale M. C., Mapelli M., Giacobbo N., Sabha N. B., Spera M., Santoliquido F., Bressan A., 2019, MNRAS, 487, 1675
Bavera S. S. et al., 2020, A&A, 635, A97
Belczynski K., Bulik T., Fryer C. L., Ruiter A., Valsecchi F., Vink J. S., Hurley J. R., 2010, ApJ, 714, 1217
Belczynski K., Holz D. E., Bulik T., O'Shaughnessy R., 2016, Nature, 534, 512
Chruslinska M., Nelemans G., Belczynski K., 2019, MNRAS, 482, 5012
Dominik M., Belczynski K., Fryer C., Holz D. E., Berti E., Bulik T., Mandel I., O'Shaughnessy R., 2013, ApJ, 779, 72
Dvorkin I., Vangioni E., Silk J., Uzan J.-P., Olive K. A., 2016, MNRAS, 461, 3877
Elbert O. D., Bullock J. S., Kaplinghat M., 2018, MNRAS, 473, 1186
Fryer C. L., Belczynski K., Wiktorowicz G., Dominik M., Kalogera V., Holz D. E., 2012, ApJ, 749, 91
Giacobbo N., Mapelli M., 2018, MNRAS, 480, 2011
Giacobbo N., Mapelli M., Spera M., 2018, MNRAS, 474, 2959
Ginolfi M., Graziani L., Schneider R., Marassi S., Valiante R., Dell'Agli F., Ventura P., Hunt L. K., 2018, MNRAS, 473, 4538
Graziani L., 2019, Physics, 1, 412
Graziani L., Salvadori S., Schneider R., Kawata D., de Bennassuti M., Maselli A., 2015, MNRAS, 449, 3137
Graziani L., de Bennassuti M., Schneider R., Kawata D., Salvadori S., 2017, MNRAS, 469, 1101
Graziani L., Schneider R., Ginolfi M., Hunt L. K., Maio U., Glatzle M., Ciardi B., 2020, MNRAS, 494, 1071
Hopkins A. M., Irwin M. J., Connolly A. J., 2001, ApJ, 558, L31
Isoyama S., Nakano H., Nakamura T., 2018, Prog. Theor. Exp. Phys., 2018, 073E01
Kalogera V. et al., 2019, Bull. Am. Astron. Soc., 51, 242
Lamberts A., Garrison-Kimmel S., Clausen D. R., Hopkins P. F., 2016, MNRAS, 463, L31
Madau P., Fragos T., 2017, ApJ, 840, 39
Maiolino R., Mannucci F., 2019, A&AR, 27, 3
Mapelli M., Giacobbo N., 2018, MNRAS, 479, 4391
Mapelli M., Colpi M., Zampieri L., 2009, MNRAS, 395, L71
Mapelli M., Ripamonti E., Zampieri L., Colpi M., Bressan A., 2010, MNRAS, 408, 234
Mapelli M., Zampieri L., Ripamonti E., Bressan A., 2013, MNRAS, 429, 2298
Mapelli M., Giacobbo N., Ripamonti E., Spera M., 2017, MNRAS, 472, 2422
Mapelli M., Giacobbo N., Santoliquido F., Artale M. C., 2019, MNRAS, 487, 2
Marassi S., Schneider R., Ferrari V., 2009, MNRAS, 398, 293
Marassi S., Schneider R., Corvino G., Ferrari V., Portegies Zwart S., 2011, Phys. Rev. D, 84, 124037
Marassi S., Graziani L., Ginolfi M., Schneider R., Mapelli M., Spera M., Alparone M., 2019, MNRAS, 484, 3219
Neijssel C. J. et al., 2019, MNRAS, 490, 3740
O'Shaughnessy R., Bellovary J. M., Brooks A., Shen S., Governato F., Christensen C. R., 2017, MNRAS, 464, 2831
Planck Collaboration VI, 2018, preprint (arXiv:1807.06209)
Portegies Zwart S. F., Verbunt F., 1996, A&A, 309, 179
Regimbau T., 2011, Res. Astron. Astrophys., 11, 369
Schneider R., Marassi S., Ferrari V., 2010, Class. Quantum Gravity, 27, 194007
Schneider R., Graziani L., Marassi S., Spera M., Mapelli M., Alparone M., de Bennassuti M., 2017, MNRAS, 471, L105
Sesana A., 2016, Phys. Rev. Lett., 116, 231102
Spera M., Mapelli M., Bressan A., 2015, MNRAS, 451, 4086
Venumadhav T., Zackay B., Roulet J., Dai L., Zaldarriaga M., 2019, preprint (arXiv:1904.07214)

This paper has been typeset from a TEX/LATEX file prepared by the author.